Nondipole Time Delay and Double-Slit Interference in Tunneling Ionization

Pei-Lun He[*], Karen Z. Hatsagortsyan[†], and Christoph H. Keitel

Max-Planck-Institut für Kernphysik, Saupfercheckweg 1, 69117 Heidelberg, Germany

Recently two-center interference in single-photon molecular ionization was employed to observe a zeptosecond time delay due to the photon propagation of the internuclear distance in a molecule [Grundmann *et al.*, Science **370**, 339 (2020)]. We investigate the possibility of a comparable nondipole time delay in tunneling ionization and decode the emerged time delay signal. With the here newly developed Coulomb-corrected nondipole molecular strong-field approximation, we derive and analyze the photoelectron momentum distribution, the signature of nondipole effects, and the role of the degeneracy of the molecular orbitals. We show that the ejected electron momentum shifts and interference fringes efficiently imprint both the molecule structure and laser parameters. The corresponding nondipole time delay value significantly deviates from that in single-photon ionization. In particular, when the two-center interference in the molecule is destructive, the time delay is independent of the bond length. We also identify the double-slit interference in tunneling ionization of atoms with nonzero angular momentum via a nondipole momentum shift.

Whether a photoelectron requires a finite nonzero time to absorb photons is a controversial question since Einstein's photoelectric effect theory. Attoscience reformulates it, featuring several types of time delays of attosecond scale [1–3]. By tuning the delay between the ionizing XUV pump pulse and the streaking infrared laser pulse, the photoemission time delay from atoms, molecules, and surfaces has been measured [4,5]. The invention of the attoclock technique [6,7] allowed us to probe the tunneling ionization time delay [8–11], deriving it from the analysis of the attoclock offset angle [12]. Recently, Mössbauer spectroscopy made it possible to control the phase delay of x-ray pulses on the zeptosecond timescale [13].

Nondipole effects in strong-field ionization recently became accessible at modest laser intensities due to the achieved high precision measurements of electron and ion momenta [14–22]. In particular, Grundmann *et al.* [23] identified a new kind of time delay in single-photon ionization of a molecule, which originates from the finiteness of the light speed. The effect is thus essentially a nondipole [24–33] ionization delay. The photon inducing the ionization arrives at the nuclei at different times. As a consequence, the photoelectron released from different sites features a zeptosecond birth time delay with respect

to both sites [23], resulting in a shift of the double-slit interference fringe in the photoelectron momentum distribution. From first-order perturbation theory based on single-photon ionization [34], one can prove that the birth time delay is the same as the delay of the light-front arriving at the two nuclei. While the two-center interference effects are usually suppressed for tunneling ionization, recently double-slit photoelectron interference has been observed in strong-field ionization for a special molecular object of the neon dimer [41], which has a large distance between the ionization centers. This rises hope to observe a comparable nondipole zeptosecond ionization time delay in molecular systems in the tunneling ionization regime [42]. Rather than using high-energy photons of the keV range for inducing ionization as in Ref. [23], the ionization here is initiated involving many photons by an intense infrared laser field and leads to different values of nondipole ionization time delay.

In this Letter, we investigate the strong-field ionization time delay of a molecule due to the finiteness of the light speed. For this purpose, we have developed a Coulomb-corrected nondipole molecular strong-field approximation (SFA) and apply it to tunneling ionization of diatomic molecules. The photoelectron momentum distribution (PMD) and its features due to nondipole interaction are examined. To uncover the nondipole ionization time delay, we additionally invoke the Wigner quasidistribution function based on the SFA transition amplitude. We deduce the photoelectron's tunneling exit distribution, i.e., its spatial density near the tunneling exit from the Wigner quasiprobability distribution. While the exit distribution is a superposition of two Gaussian functions centered at the two

nuclei, the effective distribution width determining the time delay is generally distinct from the internuclear distance. This is due to the weight factors stemming from the molecular axis-dependent ionization, the interference of the wave packets, and the exponentially decaying exit distribution factor. Thus, the time delay extracted from the PMD fringes in the nondipole tunneling ionization reflects the effective separation of the ionization centers rather than the distance between nuclei as in single-photon ionization. We analyze the best conditions and molecular systems for experimental observation of the nondipole time delay in tunneling ionization. Finally, we apply the same analysis to the tunneling ionization of an atomic bound state with nonzero angular quantum numbers and derive the comparable characteristic nondipole momentum shifts as a consequence of double-slit interference.

We consider tunneling ionization of a homonuclear molecule with the nuclei displacement $\mathbf{R}$ in a circularly polarized laser field. Our treatment is based on the Coulomb corrected nondipole SFA. The latter employs the eikonal-Volkov wave function [43–47] for the description of the continuum dynamics, and the asymptotic molecular wave function $\Psi = \sum_{l,m} C_{lm} \kappa^{\nu+1/2} r^{\nu-1} e^{-\kappa r} Y_{lm}(\mathbf{x})$ for the bound state [48,49]. The bound-state wave function is matched to the continuum eikonal wave function under the barrier and provides the dominant contribution to tunneling ionization [50–52]. Here, $\nu = Z_c/\kappa$ is the effective principal quantum number, with the effective nuclei charge Z_c, $\kappa = \sqrt{2I_p}$, and I_p the ionization energy, C_{lm} are numerical coefficients, see Refs. [48,49], and Y_{lm} spherical harmonics. For compactness of writing, we suppress the dependence of C_{lm} and I_p on $\mathbf{R}$. The light-front ionization transition amplitude [47] reads

$$M_{\mathbf{p}} = -i \int d\eta \frac{d^3\mathbf{x}}{(2\pi)^{3/2}} (1 - \tilde{p}_z/c) e^{-i \int_{\eta}^{\infty} d\eta' \frac{\frac{1}{2}\tilde{\mathbf{p}}(\eta')^2 + I_p}{1 - \frac{\tilde{p}_z}{c}}}$$
$$\times e^{-i\tilde{\mathbf{p}}(\eta)\cdot\mathbf{x}} \mathbf{x} \cdot \mathbf{E}(\eta) \Psi(\mathbf{x}) \mathcal{F}_C^*(\eta, \mathbf{x}), \qquad (1)$$

where $\mathbf{E}(\eta)$ is the electric field, $\eta = t - z/c$ the light-front time, $\mathcal{F}_C(\eta, \mathbf{x}) = \exp\{i \int_{\eta}^{\infty} d\eta' V[\mathbf{x}(\eta, \eta')]/(1 - p_-/c)\}$ the Coulomb correction factor, $\tilde{\mathbf{p}} = (\mathbf{p}_\perp, \tilde{p}_z)$ the momentum, $\tilde{p}_z = p_- - I_p/c$, $\tilde{\mathbf{p}}(\eta) = \tilde{\mathbf{p}} + \mathbf{A}(\eta)$, and $\mathbf{A}(\eta)$ the laser vector potential, and $p_- = p_z - \mathbf{p}^2/(2c)$ the light-front momentum. Employing saddle-point integration and the Coulomb matching method [34,47,53], the squared modulus of $M_{\mathbf{p}}$ gives the differential ionization rate

$$\Gamma(\eta, v_\perp, \tilde{p}_z) = F_M \frac{2^{2\nu}\kappa^{6\nu}}{(1 - \frac{\tilde{p}_z}{c})^{2\nu} E(\eta)^{2\nu}} \exp\left[-\frac{2}{3}\frac{\kappa^3}{E(\eta)(1 - \frac{\tilde{p}_z}{c})}\right]$$
$$\times \exp\left[-\frac{\kappa(v_\perp^2 + \tilde{p}_z^2)}{E(\eta)(1 - \frac{\tilde{p}_z}{c})}\right], \qquad (2)$$

where $F_M = |\sum_{l,m} C_{lm} Y_{lm}(\tilde{\mathbf{p}}(\eta_s))|^2$ is the molecular form factor, η_s the saddle point, $E(\eta) = |\mathbf{E}(\eta)|$, and $\mathbf{v}_\perp = (v_x, v_y, 0)$ the initial velocity perpendicular to the electric field in the polarization plane. Equation (2) is the nondipole generalization of the molecular Perelomov-Popov-Terent'ev (PPT) theory [48,50–52]. To extract the spatial distribution of the tunneling ionization exit, we apply the Wigner transformation [54] using the ionization amplitude Eq. (1):

$$W(\eta, v_\perp, \tilde{p}_z, z) \equiv \frac{1}{2\pi} \int_{-\infty}^{+\infty} dq JM(\eta, v_\perp, \tilde{p}_z - q/2)$$
$$\times M^*(\eta, v_\perp, \tilde{p}_z + q/2) e^{izq}, \qquad (3)$$

where $J = [E(\eta)/(1 - \tilde{p}_z/c)]$ is the Jacobian for the coordinate transformation from (p_x, p_y, p_z) to $(\eta, v_\perp, \tilde{p}_z)$. Integrating out $\tilde{p}_z$, we obtain the tunneling exit distribution

$$\hat{\Gamma}(\eta, v_\perp, z) \equiv \int d\tilde{p}_z W(\eta, v_\perp, \tilde{p}_z, z). \qquad (4)$$

Throughout the Letter, all PMDs and exit distributions are calculated using Eqs. (2) and (4), respectively.

We use H_2^+ molecule as a prototype, whose ground and excited states are nondegenerate. Approximating the wave function by the linear combination of atomic orbitals $\Psi \propto e^{-\kappa|\mathbf{x}-\mathbf{R}/2|} \pm e^{-\kappa|\mathbf{x}+\mathbf{R}/2|}$, the form factor reads

$$F_M \propto \cosh\alpha \pm \cos\tilde{\beta}, \qquad (5)$$

where $\tilde{\beta} = \mathbf{R} \cdot \mathbf{v}_i$, $\mathbf{v}_i = (v_x, v_y, \tilde{p}_z)$ is the initial momentum, and $\alpha = \kappa[(\mathbf{E} \cdot \mathbf{R})/E]$. The $\pm$ corresponds to σ_g $1s$ and σ_u $1s$ states, respectively. From the exit distribution $\hat{\Gamma}(\eta, v_\perp, z) = |A(\eta, v_\perp, z)|^2$, we find the amplitudes of ionization emerging from the nuclei:

$$A(\eta, v_\perp, z) \propto e^{\frac{\alpha}{2}} \exp\left[-\frac{1}{2R_w^2}\left(z - \frac{R_z}{2}\right)^2 - i\frac{1}{2}\beta\right]$$
$$\pm e^{-\frac{\alpha}{2}} \exp\left[-\frac{1}{2R_w^2}\left(z + \frac{R_z}{2}\right)^2 + i\frac{1}{2}\beta\right], \quad (6)$$

where $\beta = \mathbf{R} \cdot \mathbf{v}_\perp$, and $R_w = \sqrt{[\kappa/E(\eta)]}$. The emitted photoelectron wave packets are centered at $z = \pm R_z/2$. However, due to the rather significant width R_w of the exit distribution, and moreover, the unequal weights of the two nuclei (as the ionization from the uphill nucleus at the position $(\alpha/|\alpha|)(\mathbf{R}/2)$ is preferred [55,56]), the effective separation of the tunneling exits differs from R_z. The effective separation of the ionization bursts depends on the molecular form factor and is essentially different in the case of nondegenerate or degenerate molecular orbitals. For the nondegenerate molecular orbitals as in H_2^+, one center contribution, which has a large factor $\propto e^\alpha$, is dominant.
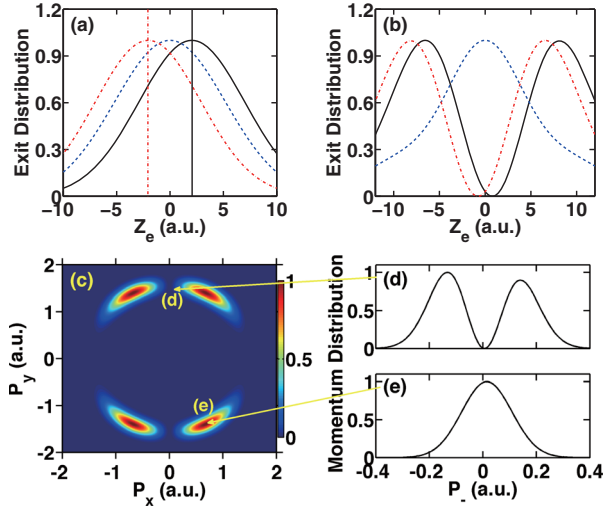
FIG. 1. Tunneling exit distribution when the molecular axis angle is $\theta_m = \pi/4$: (a) for H_2^+ with nondegenerate molecular orbitals $(\sigma_g 1s)$, where the vertical lines mark the position $z_e = \pm R_z/2$; (b) Ne_2 with degenerate molecular orbitals $(\sigma_g 2p)$; in (a),(b) the ionization phase is $\Phi = 0$ (black solid), $\Phi = \pi/2$ (blue dashed), and $\Phi = \pi$ (red dotted-dashed); (c) PMD of Ne_2 $(\sigma_g 2p)$ in the polarization plane. The dark fringe (d) has double peaks, while the bright fringe (e) has a single peak in the longitudinal PMD. The probability of the dark fringe is 10 times smaller than the bright one. The laser vector potential is $\mathbf{A}(\eta) = -A_0(\sin\Phi, \cos\Phi, 0)$ with wavelength 3000 nm and intensity $I = 4 \times 10^{13}$ W/cm^2; $\mathbf{R} = R(\sin\theta_m, 0, \cos\theta_m)$.

The tunneling exit distribution in this case is shown in Fig. 1(a) for the molecular axis angle $\theta_m = \pi/4$. It is a Gaussian distribution centered at the uphill nucleus. Therefore, the two-center interference is suppressed. Note that the bond length and the axis orientation can be retrieved by measuring the correlated nuclei kinetic energy release [41,57,58].

In the case of degenerate molecular orbitals, such as in rare gas dimers, the initial bound state is dressed by the laser field [59,60]. Two nuclei $\pm\frac{1}{2}\mathbf{R}$ have the same weight but acquire different phase factors $e^{\pm i\frac{1}{2}\mathbf{A}\cdot\mathbf{R}}$. For He_2 as an example, we have $\Psi \propto e^{i\frac{1}{2}\mathbf{A}\cdot\mathbf{R}}e^{-\kappa|\mathbf{x}-\mathbf{R}/2|} \pm e^{-i\frac{1}{2}\mathbf{A}\cdot\mathbf{R}}e^{-\kappa|\mathbf{x}+\mathbf{R}/2|}$, such that the molecular form factor is

$$F_M \propto (1 \pm \cos \mathbf{R} \cdot \tilde{\mathbf{p}}), \tag{7}$$

and the tunneling exit distribution is described by Eq. (6) with $\alpha = 0$. Depending on the phase $\mathbf{A} \cdot \mathbf{R}$, the ionization signal from two nuclei can interfere constructively or destructively. Thus, the exit distribution switches from a single peak distribution centered at $z_e = 0$ to double peaks at $z_e = \pm R_w$. For the latter, we have two separated contributions, equal in the probability [Fig. 1(b)]. The emergence of two exits in tunneling ionization can be seen in the PMD in the laser polarization plane, as the appearance of interference fringes for Ne_2 [Fig. 1(c)] in contrast to the case N_2, see

Refs. [34,41]. The bright fringe in Fig. 1(c) is created at the laser phase $\Phi = 3\pi/4$ with a high probability and corresponds to the single exit case [Fig. 1(b)]. Accordingly, the longitudinal PMD for the bright transverse fringe exhibits a single peak [Fig. 1(e)]. However, the dark fringes are created via double exit contributions at the laser phases $\Phi = 0, \pi$, and feature the double-peak structure in the longitudinal PMD [Fig. 1(d)]. As the probability of dark fringes is 10 times smaller than that of bright ones, the experimental observation is challenging.

We underline that the exit distribution [Eq. (4)] in the nondipole regime is derived at a given light-front time (corresponding to the real part of the ionization saddle point via the η variable) $\eta_e = t_e - z_e/c$, where the sublabel e stands for the tunneling exit. This means that the coordinates of two peaks of the exit distribution $z_{e1,2}$ are related to different time moments $t_{e1,2} = \eta_e + z_{e1,2}/c$, which implies a time delay $\Delta t_e = \Delta z_e/c$, with $\Delta z_e = z_{e2} - z_{e1}$. Thus, in molecular tunneling ionization, the nondipole time delay is determined by the distance between the tunneling exits rather than the bond length as in single-photon ionization. The exit distribution is gauge independent as determined by the gauge-invariant quantities of the molecular form factor F_M and the width R_w. In principle, the nondipole ionization time delay could be observed directly in a pump-probe experiment [34].

The nondipole time delay Δt_e results in an interference fringe shift. Wave packets emitted from the exit $\mathbf{x}_e$ acquire the phase $\phi = \mathbf{p} \cdot (\mathbf{x} - \mathbf{x}_e) - E_{\mathbf{p}}(t - t_e) + I_p t_e$. The phase difference $\Delta\phi$ determines the interference: $\Delta\phi = \mathbf{p}_\perp \cdot \Delta\mathbf{x}_{e\perp} + p_z \Delta z_e - (E_{\mathbf{p}} + I_p)\Delta t_e = \mathbf{p}_\perp \cdot \Delta\mathbf{x}_{e\perp} + (p_- - I_p/c)\Delta z_e$, where $\Delta\mathbf{x}_{e\perp}$ denotes the difference of the exit transverse coordinates. Because of the nondipole time delay (the $1/c$-term in $\Delta\phi$), the main fringe shifts from $p_z = 0$ to $p_- = I_p/c$. The above analysis is verified by the dark fringe shift in the inset of Fig. 2(e), which in turn confirms the time delay conjecture $\Delta t_e = \Delta z_e/c$. There is an analogy in the interpretation of the interference fringe shift as a time delay for single-photon ionization [23,30] and strong-field ionization. The shift in both cases originates from the wave propagating time through the distance Δz between the two ionization centers and is given by the phase difference term $(E_{\mathbf{p}} + I_p)\Delta z/c = \delta\varepsilon\Delta z/c$, with the laser energy $\delta\varepsilon$ absorbed in the process. In single-photon ionization, $\delta\varepsilon$ is the absorbed high-frequency photon energy and $\Delta z = R_z$. While in tunneling ionization $\delta\varepsilon \sim I_p + U_p$, where the ponderomotive potential U_p is due to the multiphoton process and $\Delta z = \Delta z_e$.

Because of the position-momentum duality, the separation of momentum interference fringes is $\Delta p_- \approx 2\pi/\Delta z_e$. Let us analyze the exit and momentum distributions at different internuclear distances for the case of degenerate molecular orbitals on the example of He_2. Because of its weak binding energy, the bound state of He_2 has a halo structure, and the bond length has a wide distribution
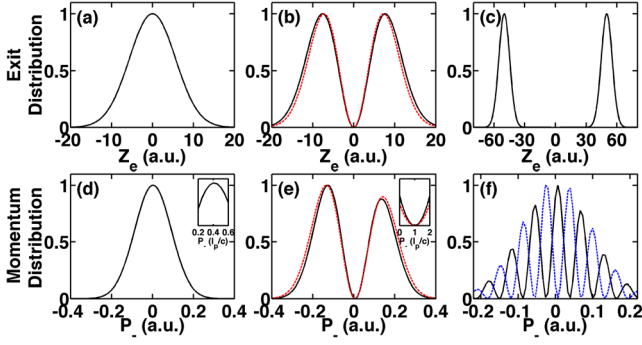
FIG. 2. The tunneling exit and longitudinal momentum distributions for He$_2$ with degenerate molecular orbitals, with the molecular axis angle $\theta_m = 0$: (a)–(c) Exit distribution; (d)–(f) Longitudinal PMD; (a,d) for the electronic state σ_g $1s$ with $R = 5$ a.u.; (b),(e) for the state σ_u $1s$ with $R = 5$ a.u. (black); for the atom with ($l = 1$, $m = 0$) (red); (c),(f) for σ_g $1s$ (black), and σ_u $1s$ (blue), with $R = 100$ a.u. Laser parameters are the same as in Fig. 1. The inset is the enlargement around $p_- = I_p/c$. The nondipole shift of the dark fringe in PMD is I_p/c.

[61–63]. Both the interference effect and the decay width R_w are vital here. We consider the case of $\theta_m = 0$, when the exit distribution is independent of the laser phase. For $R = 5$ a.u., the exit distribution of the σ_g $1s$ state has a single peak described by a Gaussian. Consequently, there is no two-center interference, and PMD also has a Gaussian form [Figs. 2(a) and 2(d)]. In contrast, the exit distribution of the σ_u $1s$ state has two peaks at $z = \pm R_w$, which yields a two peak structure in PMD with a separation of $\Delta p_- = 2/R_w$ [Figs. 2(b) and 2(e)]. When the distance between the molecular centers is much larger than the width R_w, for instance, $R = 100$ a.u. [Figs. 2(c) and 2(f)], the exit separation coincides with the molecular center separation. In fact, the exit has two peaks at $z_e = \pm R/2$ in Fig. 2(c), which results in multiple peaks PMD with a peak separation of $\Delta p_- = 2\pi/R$ [Fig. 2(f)]. Thus, the interference structure from PMD of He$_2$ features a fringe separation according to the effective distance between the two tunneling exits Δz_e.

In the experiment, it is convenient to measure the signature of nondipole effects in the average longitudinal momentum shift $\langle p_- \rangle \sim I_p/c$. The signature is robust against continuum Coulomb corrections [34]. It contains nonnegligible molecular contribution additional to the atomic $I_p/(3c)$ [17,24], $\delta\langle p_- \rangle \equiv \langle p_- \rangle - I_p/(3c)$, which depends on molecular parameters R_z, $R_\perp$, and R_w. In Fig. 3, we show $\delta\langle p_- \rangle$ as a function of molecular orientation. The shift for H$_2^+$ is calculated using Eqs. (2) and (5) as

$$\langle p_- \rangle = \frac{I_p}{3c}\left[1 + \frac{(R_z^2/R_w^2)}{1 \pm \exp(\frac{R_z^2}{4R_w^2})I_0(\kappa R_\perp)}\right], \qquad (8)$$

where $\pm$ corresponds to the σ_g $1s$ and σ_u $1s$ state, respectively, $R_\perp = \sqrt{R^2 - R_z^2}$, and $I_0(x)$ is the modified
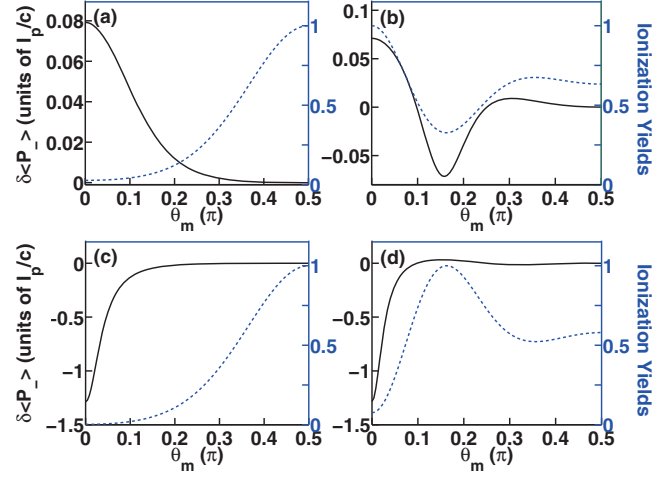
FIG. 3. Nondipole momentum shift $\delta\langle p_- \rangle$ (black solid lines) due to the molecular contribution and the ionization yield (blue dashed lines) vs molecular axis angle θ_m: (a),(b) Ionization from σ_g $1s$; (c),(d) Ionization from σ_u $1s$; (a),(c) Ionization of H$_2^+$; (b),(d) Ionization of He$_2$; Laser parameters are the same as in Fig. 1; $\mathbf{R} = R(\sin\theta_m, 0, \cos\theta_m)$, $R = 5$ a.u.

Bessel function of the first kind. The ionization is dominated by the instant when the electric field is parallel to the molecule axis. When $R_z \gg R_w$, the molecular contribution is exponentially suppressed. At $R_z \sim R_w$ there is a significant molecular contribution in $\delta\langle p_- \rangle$ when $\theta_m \ll 1$ [Figs. 3(a) and 3(c)], however, in this case the ionization yield is suppressed (the case $\theta_m = 0$ is discussed in Ref. [42]). Thus, a H$_2^+$ molecule with nondegenerate orbitals is not beneficial for observing the molecule-specific nondipole momentum shift.

For He$_2$ with degenerate orbitals and the molecular form factor Eq. (7), the nondipole longitudinal momentum shift is

$$\langle p_- \rangle = \frac{I_p}{3c}\left[1 + \frac{(R_z^2/R_w^2)J_0(A_0 R_\perp)}{J_0(A_0 R_\perp) \pm \exp\frac{R_z^2}{4R_w^2}}\right], \qquad (9)$$

where $J_0(x)$ is the Bessel function of the first kind. In this case the molecular nondipole momentum shift can be observed at intermediate θ_m for the case of degenerate orbitals with an appreciable yield, see Figs. 3(b) and 3(d). The minima of the solid lines are due to the destructive double-slit interference, which suppresses the ionization yields. Its appearance implies more nodes in Fig. 1(c), with a two-peak longitudinal distribution [Fig. 1(d)] and a negative contribution to the total momentum shift. As a consequence, the momentum shift also has a local minimum at this θ_m.

So far, we have interpreted the nondipole momentum shift as a consequence of the time delay of the driving laser arriving at the two exits for molecules. The same interpretation is valid for an atom with an angular momentum of

$(l, m) = (1, 0)$, where again two tunneling exits exists, given by the following tunneling exit distribution:

$$\hat{\Gamma}(\eta, v_\perp, z) \propto \frac{z^2}{R_w^2} \exp\left(-R_w^2 v_\perp^2 - \frac{z^2}{R_w^2}\right). \quad (10)$$

This distribution has two peaks at $z = \pm R_w$ with opposite phases. The interference of the wave packets emitted from two effective centers is thus identical to the σ_u 1s molecule with $\theta_m = 0$ [Figs. 2(b) and 2(e)]. The two exit peaks at $z = \pm R_w$ with opposite phases imply two momentum peaks at $\tilde{p}_z = \pm 1/R_w$. Considering the weight of the two peaks [34], we have the average momentum shift as $\langle p_- \rangle = -I_p/c$, which coincides with the known result [47]. Thus, the nondipole momentum shift for the atom in this case is due to a time delay of the laser wave traveling the distance between the two exits: $\Delta t_e = 2R_w/c$.

Concluding, we have investigated the nondipole strong-field ionization time delay due to the finiteness of the light speed and find that the delay depends essentially on the tunneling exit distribution, rather than the molecular bond length. We show also that the tunneling exit distribution of an atom with a nonzero angular momentum features two tunneling exits, which yields a nontrivial time delay as a consequence of destructive double-slit interference. The nondipole ionization delay manifests itself in the longitudinal momentum distribution, which efficiently imprints the molecule structure and laser parameters. For rare gas dimers, the bright fringe in the polarization plane has a single longitudinal peak ($\Delta t_e = 0$), while the dark fringe has double longitudinal peaks ($\Delta t_e = (2R_w/c)$). For dissociated molecules with $R \gg R_w$, the longitudinal momentum distribution has multiple peaks ($\Delta t_e = (R_z/c)$). Our analysis could be extended to more complex molecules, where richer forms of nondipole time delays are expected.

*peilun@mpi-hd.mpg.de
†k.hatsagortsyan@mpi-hd.mpg.de

[1] P. B. Corkum and F. Krausz, Attosecond science, Nat. Phys. **3**, 381 (2007).

[2] P. H. Bucksbaum, The future of attosecond spectroscopy, Science **317**, 766 (2007).

[3] F. Krausz and M. Ivanov, Attosecond physics, Rev. Mod. Phys. **81**, 163 (2009).

[4] A. Maquet, J. Caillat, and R. Taïeb, Attosecond delays in photoionization: Time and quantum mechanics, J. Phys. B **47**, 204004 (2014).

[5] R. Pazourek, S. Nagele, and J. Burgdörfer, Attosecond chronoscopy of photoemission, Rev. Mod. Phys. **87**, 765 (2015).

[6] C. M. Maharjan, A. S. Alnaser, X. M. Tong, B. Ulrich, P. Ranitovic, S. Ghimire, Z. Chang, I. V. Litvinyuk, and C. L. Cocke, Momentum imaging of doubly charged ions of ne and ar in the sequential ionization region, Phys. Rev. A **72**, 041403(R) (2005).

[7] P. Eckle, M. Smolarski, F. Schlup, J. Biegert, A. Staudte, M. Schöffler, H. G. Muller, R. Dörner, and U. Keller, Attosecond angular streaking, Nat. Phys. **4**, 565 (2008).

[8] P. Eckle, A. N. Pfeiffer, C. Cirelli, A. Staudte, R. Dörner, H. G. Muller, M. Büttiker, and U. Keller, Attosecond ionization and tunneling delay time measurements in helium, Science **322**, 1525 (2008).

[9] A. N. Pfeiffer, C. Cirelli, M. Smolarski, D. Dimitrovski, M. Abu-samha, L. B. Madsen, and U. Keller, Attoclock reveals natural coordinates of the laser-induced tunnelling current flow in atoms, Nat. Phys. **8**, 76 (2012).

[10] N. Camus, E. Yakaboylu, L. Fechner, M. Klaiber, M. Laux, Y. Mi, K. Z. Hatsagortsyan, T. Pfeifer, C. H. Keitel, and R. Moshammer, Experimental Evidence for Wigner's Tunneling Time, Phys. Rev. Lett. **119**, 023201 (2017).

[11] U. S. Sainadh, H. Xu, X. Wang, A. Atia-Tul-Noor, W. C. Wallace, N. Douguet, A. W. Bray, I. Ivanov, K. Bartschat, A. Kheifets, R. T. Sang, and I. V. Litvinyuk, Attosecond angular streaking and tunnelling time in atomic hydrogen, Nature (London) **568**, 75 (2019).

[12] A. S. Landsman and U. Keller, Attosecond science and the tunnelling time problem, Phys. Rep. **547**, 1 (2015).

[13] K. P. Heeg, A. Kaldun, C. Strohm, C. Ott, R. Subramanian, D. Lentrodt, J. Haber, H.-C. Wille, S. Goerttler, R. Rüffer et al., Coherent x-ray- optical control of nuclear excitons, Nature (London) **590**, 401 (2021).

[14] C. T. L. Smeenk, L. Arissian, B. Zhou, A. Mysyrowicz, D. M. Villeneuve, A. Staudte, and P. B. Corkum, Partitioning of the Linear Photon Momentum in Multiphoton Ionization, Phys. Rev. Lett. **106**, 193002 (2011).

[15] A. Ludwig, J. Maurer, B. W. Mayer, C. R. Phillips, L. Gallmann, and U. Keller, Breakdown of the Dipole Approximation in Strong-Field Ionization, Phys. Rev. Lett. **113**, 243001 (2014).

[16] J. Maurer, B. Willenberg, J. Daněk, B. W. Mayer, C. R. Phillips, L. Gallmann, M. Klaiber, K. Z. Hatsagortsyan, C. H. Keitel, and U. Keller, Probing the ionization wave packet and recollision dynamics with an elliptically polarized strong laser field in the nondipole regime, Phys. Rev. A **97**, 013404 (2018).

[17] A. Hartung, S. Eckart, S. Brennecke, J. Rist, D. Trabert, K. Fehre, M. Richter, H. Sann, S. Zeller, K. Henrichs et al., Magnetic fields alter strong-field ionization, Nat. Phys. **15**, 1222 (2019).

[18] B. Willenberg, J. Maurer, B. W. Mayer, and U. Keller, Sub-cycle time resolution of multi-photon momentum transfer in strong-field ionization, Nat. Commun. **10**, 5548 (2019).

[19] N. Haram, I. Ivanov, H. Xu, K. T. Kim, A. Atia-tul Noor, U. S. Sainadh, R. D. Glover, D. Chetty, I. V. Litvinyuk, and R. T. Sang, Relativistic Nondipole Effects in Strong-Field Atomic Ionization at Moderate Intensities, Phys. Rev. Lett. **123**, 093201 (2019).

[20] A. Hartung, S. Brennecke, K. Lin, D. Trabert, K. Fehre, J. Rist, M. S. Schöffler, T. Jahnke, L. P. H. Schmidt, M. Kunitski, M. Lein, R. Dörner, and S. Eckart, Electric Nondipole Effect in Strong-Field Ionization, Phys. Rev. Lett. **126**, 053202 (2021).

[21] K. Lin, S. Brennecke, H. Ni, X. Chen, A. Hartung, D. Trabert, K. Fehre, J. Rist, X.-M. Tong, J. Burgdörfer, L. P. H. Schmidt, M. S. Schoffler, T. Jahnke, M. Kunitski, F. He, M. Lein, S. Eckart, and R. Dorner, Magnetic-Field Effect in High-Order Above-Threshold Ionization, Phys. Rev. Lett. **128,** 023201 (2022).

[22] K. Lin, S. Eckart, A. Hartung, D. Trabert, K. Fehre, J. Rist, L. P. H. Schmidt, M. S. Schöffler, T. Jahnke, M. Kunitski, and R. Dörner, Photoelectron energy peaks shift against the radiation pressure in strong field ionization, arXiv: 2110.04027.

[23] S. Grundmann, D. Trabert, K. Fehre, N. Strenger, A. Pier, L. Kaiser, M. Kircher, M. Weller, S. Eckart, L. P. H. Schmidt, F. Trinter, T. Jahnke, M. S. Schöffler, and R. Dörner, Zeptosecond birth time delay in molecular photoionization, Science **370,** 339 (2020).

[24] M. Klaiber, E. Yakaboylu, H. Bauke, K. Z. Hatsagortsyan, and C. H. Keitel, Under-the-Barrier Dynamics in Laser-Induced Relativistic Tunneling, Phys. Rev. Lett. **110,** 153004 (2013).

[25] S. Chelkowski, A. D. Bandrauk, and P. B. Corkum, Photon Momentum Sharing Between an Electron and an Ion in Photoionization: From One-Photon (Photoelectric Effect) to Multiphoton Absorption, Phys. Rev. Lett. **113,** 263005 (2014).

[26] D. Lao, P.-L. He, and F. He, Longitudinal photoelectron momentum shifts induced by absorbing a single xuv photon in diatomic molecules, Phys. Rev. A **93,** 063403 (2016).

[27] P.-L. He, D. Lao, and F. He, Strong Field Theories Beyond Dipole Approximations in Nonrelativistic Regimes, Phys. Rev. Lett. **118,** 163203 (2017).

[28] S. Chelkowski and A. D. Bandrauk, Photon momentum transfer in photoionisation: Unexpected breakdown of the dipole approximation, Mol. Phys. **115,** 1971 (2017).

[29] Z.-H. Zhang and F. He, Photoionization of h_2^+ beyond the dipole approximation with zeptosecond time resolution, Phys. Rev. A **103,** 033112 (2021).

[30] I. A. Ivanov, A. S. Kheifets, and K. T. Kim, Effect of the finite speed of light in ionization of extended molecular systems, Sci. Rep. **11,** 21457 (2021).

[31] H. Liang, S. Grundmann, Y.-K. Fang, L. Geng, Q. Gong, and L.-Y. Peng, Nondipole effects in interference patterns of a two-electron wave, Phys. Rev. A **104,** L021101 (2021).

[32] K. Liu, Y. Hu, Q. Zhang, and P. Lu, Nondipole effects on the double-slit interference in molecular ionization by xuv pulses, Opt. Express **29,** 38758 (2021).

[33] X. Y. Lai, S. P. Xu, S. G. Yu, M. W. Shi, W. Quan, and X. J. Liu, Revealing the wave-function-dependent zeptosecond birth time delay in molecular photoionization with double-slit interference minima, Phys. Rev. A **104,** 043105 (2021).

[34] See Supplemental Material http://link.aps.org/supplemental/10.1103/PhysRevLett.128.183201 for the details, which includes Ref. [35–40].

[35] P.-L. He and F. He, Ionization of H_2^+ in xuv pulses, Phys. Scr. **90,** 045402 (2015).

[36] L. Keldysh, Ionization in the field of a strong electromagnetic wave, Sov. Phys. JETP **20,** 1307 (1965).

[37] F. H. M. Faisal, Multiple absorption of laser photons by atoms, J. Phys. B **6,** L89 (1973).

[38] H. R. Reiss, Effect of an intense electromagnetic field on a weakly bound system, Phys. Rev. A **22,** 1786 (1980).

[39] P.-L. He, Z.-H. Zhang, and F. He, Young's Double-Slit Interference in a Hydrogen Atom, Phys. Rev. Lett. **124,** 163201 (2020).

[40] K. Liu and I. Barth, Identifying the Tunneling site in Strong-Field Ionization of H_2^+, Phys. Rev. Lett. **119,** 243204 (2017).

[41] M. Kunitski, N. Eicke, P. Huber, J. Köhler, S. Zeller, J. Voigtsberger, N. Schlott, K. Henrichs, H. Sann, F. Trinter *et al.*, Double-slit photoelectron interference in strong-field ionization of the neon dimer, Nat. Commun. **10,** 1 (2019).

[42] S. Chelkowski and A. D. Bandrauk, Photon-momentum transfer in molecular photoionization, Phys. Rev. A **97,** 053401 (2018).

[43] J. I. Gersten and M. H. Mittleman, Eikonal theory of charged-particle scattering in the presence of a strong electromagnetic wave, Phys. Rev. A **12,** 1840 (1975).

[44] O. Smirnova, M. Spanner, and M. Ivanov, Analytical solutions for strong field-driven atomic and molecular one- and two-electron continua and applications to strong-field problems, Phys. Rev. A **77,** 033407 (2008).

[45] M. Klaiber, E. Yakaboylu, and K. Z. Hatsagortsyan, Above-threshold ionization with highly charged ions in superstrong laser fields. i. Coulomb-corrected strong-field approximation, Phys. Rev. A **87,** 023417 (2013).

[46] M. Klaiber, E. Yakaboylu, and K. Z. Hatsagortsyan, Above-threshold ionization with highly charged ions in superstrong laser fields. ii. relativistic coulomb-corrected strong-field approximation, Phys. Rev. A **87,** 023418 (2013).

[47] P.-L. He, M. Klaiber, K. Z. Hatsagortsyan, and C. H. Keitel, Nondipole coulomb sub-barrier ionization dynamics and photon momentum sharing, Phys. Rev. A **105,** L031102 (2022).

[48] X. M. Tong, Z. X. Zhao, and C. D. Lin, Theory of molecular tunneling ionization, Phys. Rev. A **66,** 033402 (2002).

[49] S.-F. Zhao, C. Jin, A.-T. Le, T. F. Jiang, and C. D. Lin, Determination of structure parameters in strong-field tunneling ionization theory of molecules, Phys. Rev. A **81,** 033423 (2010).

[50] A. M. Perelomov, V. S. Popov, and M. V. Terent'ev, Ionization of atoms in an alternating electric field, Sov. Phys. JETP **23,** 924 (1966).

[51] A. M. Perelomov and V. S. Popov, Ionization of atoms in an alternating electric field. III, Sov. Phys. JETP **25,** 336 (1967).

[52] M. V. Ammosov, N. B. Delone, and V. P. Krainov, Tunnel ionization of complex atoms and of atomic ions in an alternating electromagnetic field, Zh. Eksp. Teor. Fiz. **91,** 2008 (1986).

[53] V. S. Popov, V. D. Mur, and B. M. Karnakov, The imaginary-time method for relativistic problems, Sov. Phys. JETP Lett. **66,** 229 (1997).

[54] E. Wigner, On the quantum correction for thermodynamic equilibrium, Phys. Rev. **40,** 749 (1932).

[55] T. Zuo and A. D. Bandrauk, Charge-resonance-enhanced ionization of diatomic molecular ions by intense lasers, Phys. Rev. A **52,** R2511 (1995).

[56] J. Wu, M. Meckel, L. P. H. Schmidt, M. Kunitski, S. Voss, H. Sann, H. Kim, T. Jahnke, A. Czasch, and R. Dörner, Probing the tunnelling site of electrons in strong field enhanced ionization of molecules, Nat. Commun. **3,** 1 (2012).

[57] X. Gong, P. He, Q. Song, Q. Ji, K. Lin, W. Zhang, P. Lu, H. Pan, J. Ding, H. Zeng *et al.*, Pathway-resolved photo-electron emission in dissociative ionization of molecules, Optica **3**, 643 (2016).

[58] S. Zeller, M. Kunitski, J. Voigtsberger, M. Waitz, F. Trinter, S. Eckart, A. Kalinin, A. Czasch, L. P. H. Schmidt, T. Weber, M. Schöffler, T. Jahnke, and R. Dörner, Determination of Interatomic Potentials of He_2, Ne_2, Ar_2, and H_2 by Wave Function Imaging, Phys. Rev. Lett. **121**, 083002 (2018).

[59] W. Becker, J. Chen, S. G. Chen, and D. B. Milošević, Dressed-state strong-field approximation for laser-induced molecular ionization, Phys. Rev. A **76**, 033403 (2007).

[60] C. Zhang, T. Feng, N. Raabe, and H. Rottke, Strong-field ionization of xenon dimers: The effect of two-equivalent-center interference and of driving ionic transitions, Phys. Rev. A **97**, 023417 (2018).

[61] M. Przybytek, W. Cencek, J. Komasa, G. Łach, B. Jeziorski, and K. Szalewicz, Relativistic and Quantum Electrodynamics Effects in the Helium Pair Potential, Phys. Rev. Lett. **104**, 183003 (2010).

[62] S. Zeller, M. Kunitski, J. Voigtsberger, A. Kalinin, A. Schottelius, C. Schober, M. Waitz, H. Sann, A. Hartung, T. Bauer *et al.*, Imaging the He_2 quantum halo state using a free electron laser, Proc. Natl. Acad. Sci. U.S.A. **113**, 14651 (2016).

[63] M. Kunitski, Q. Guan, H. Maschkiwitz, J. Hahnenbruch, S. Eckart, S. Zeller, A. Kalinin, M. Schöffler, L. P. H. Schmidt, T. Jahnke *et al.*, Ultrafast manipulation of the weakly bound helium dimer, Nat. Phys. **17**, 174 (2021).